

# Accelerated inference on accelerated cosmic expansion: New constraints on axionlike early dark energy with DESI BAO and ACT DR6 CMB lensing

Frank J. Qu<sup>1,2,\*</sup>, Kristen M. Surrao<sup>3,†</sup>, Boris Bolliet<sup>4,2,‡</sup>, J. Colin Hill<sup>3</sup>, Blake D. Sherwin<sup>1,2</sup>, Hidde T. Jense<sup>5</sup> and Adrien La Posta<sup>6</sup>

<sup>1</sup>*DAMTP, Centre for Mathematical Sciences, Wilberforce Road, Cambridge CB3 0WA, United Kingdom*

<sup>2</sup>*Kavli Institute for Cosmology, University of Cambridge, Madingley Road, Cambridge CB3 0HA, United Kingdom*

<sup>3</sup>*Department of Physics, Columbia University, New York, New York 10027, USA*

<sup>4</sup>*Cavendish Laboratory, Astrophysics Group, J. J. Thomson Avenue, Cambridge CB3 0HE, United Kingdom*

<sup>5</sup>*School of Physics and Astronomy, Cardiff University, The Parade, Cardiff, Wales CF24 3AA, United Kingdom*

<sup>6</sup>*Department of Physics, Denys Wilkinson Building, University of Oxford, Keble Road, Oxford OX1 3RH, United Kingdom*



(Received 10 May 2024; accepted 21 May 2025; published 6 June 2025)

The early dark energy (EDE) extension to  $\Lambda$  cold dark matter ( $\Lambda$ CDM) has been proposed as a candidate scenario to resolve the ‘‘Hubble tension.’’ We present new constraints on the EDE model by incorporating new data from the Dark Energy Spectroscopic Instrument (DESI) baryon acoustic oscillation (BAO) survey and cosmic microwave background (CMB) lensing measurements from the Atacama Cosmology Telescope (ACT) sixth data release and Planck NPIPE data. We do not find evidence for EDE. The maximum fractional contribution of EDE to the total energy density is  $f_{\text{EDE}} < 0.091$  [95% confidence level (CL)] from our baseline combination of Planck CMB, CMB lensing, and DESI BAO. Our strongest constraints on EDE come from the combination of Planck CMB and CMB lensing alone, yielding  $f_{\text{EDE}} < 0.070$  (95%CL). We also explore extensions of  $\Lambda$ CDM beyond the EDE parameters by treating the total neutrino mass as a free parameter, finding  $\sum m_\nu < 0.096$  eV (95%CL) and  $f_{\text{EDE}} < 0.087$  (95%CL). For the first time in EDE analyses, we perform Bayesian parameter estimation using neural network emulators of cosmological observables, which are on the order of 100 times faster than full Boltzmann solutions.

DOI: [10.1103/xhh6-9v62](https://doi.org/10.1103/xhh6-9v62)

## I. INTRODUCTION

One of the key parameters in cosmology, the Hubble constant  $H_0$ , has been determined with increasing precision from recent observational advances. On one hand, its value can be measured using indirect techniques, which depend on the assumption of a cosmological model. On the other hand,

its value can be determined using direct local probes that are, to a large extent, free of these assumptions (with the caveat that it is assumed that these local probes are well behaved at very low redshifts). The standard cosmological model,  $\Lambda$  cold dark matter ( $\Lambda$ CDM), predicts a value for  $H_0$  based on observations of the cosmic microwave background (CMB), e.g., from Planck [1], of  $67.5 \pm 0.5$  km s<sup>-1</sup> Mpc<sup>-1</sup>. However, direct measurements of  $H_0$  using Cepheid-calibrated type Ia supernovae (SNIa) by the SHOES Collaboration [2] result in a higher  $H_0 = 73.17 \pm 0.86$  km s<sup>-1</sup> Mpc<sup>-1</sup>, resulting in a  $5\sigma$  tension with predictions based on  $\Lambda$ CDM, in what is commonly referred to as the Hubble tension. Reference [3] discusses this tension in more detail, and Ref. [4] reviews some of the attempts that have been made to resolve it. Other local  $H_0$  measurements have included those from the tip of the red giant branch (TRGB), giving  $H_0 = 69.8 \pm 0.6$  stat  $\pm 1.6$  sys km s<sup>-1</sup> Mpc<sup>-1</sup> [5],  $H_0 = 73.22 \pm 2.06$  km s<sup>-1</sup> Mpc<sup>-1</sup> [6], and the *Hubble*

\*Contact author: [jq247@cantab.ac.uk](mailto:jq247@cantab.ac.uk)

†Contact author: [k.surrao@columbia.edu](mailto:k.surrao@columbia.edu)

‡Contact author: [bb667@cam.ac.uk](mailto:bb667@cam.ac.uk)

Published by the American Physical Society under the terms of the [Creative Commons Attribution 4.0 International license](https://creativecommons.org/licenses/by/4.0/). Further distribution of this work must maintain attribution to the author(s) and the published article’s title, journal citation, and DOI.

Space Telescope Key Project, giving  $H_0 = 71 \pm 2 \text{ stat} \pm 6 \text{ sys km s}^{-1} \text{ Mpc}^{-1}$  [7]. See Ref. [8] for a review on local, direct measurements.

Many attempts to resolve the Hubble tension involve scenarios beyond the  $\Lambda$ CDM model that increase the value of  $H_0$  inferred from indirect probes. In this work, we revisit the early dark energy (EDE) model using new data from the Dark Energy Spectroscopic Instrument (DESI) baryon acoustic oscillation (BAO) survey and CMB lensing data from the Atacama Cosmology Telescope (ACT) and Planck public release 4 (PR4). The EDE model (for reviews, see, e.g., [9,10]) falls into the category of those that reduce the size of the sound horizon. In this model, a new field is introduced just before recombination to briefly accelerate the expansion relative to  $\Lambda$ CDM that decreases the sound horizon at recombination, consequently increasing  $H_0$  in the fits to CMB data and alleviating the  $H_0$  tension [11–14]. We focus on the axionlike EDE model, specified by the axionlike potential of the form [11,15]

$$V(\phi) = m^2 f^2 (1 - \cos(\phi/f))^n.$$

Following previous data analyses (e.g., [16–20]), we restrict our analysis to integer  $n = 3$ , with  $n$  being the power-law index of the EDE potential and  $m$  the mass of the field.

We parametrize this EDE model using effective parameters following the approach of, e.g., [11,15,20]. These parameters are given by the redshift  $z_c$  at which EDE makes its largest fractional contribution  $f_{\text{EDE}}$  to the total cosmic energy budget,

$$f_{\text{EDE}}(z_c) = 8\pi G \rho_{\text{EDE}}(z_c) / (3H^2(z_c)),$$

and the initial field displacement  $\theta_i \equiv \phi_i/f$ , where  $f$  is the decay constant.

The presence of EDE impacts the physics of both the primary CMB and the CMB lensing power spectrum. As detailed in [21], the background effect of EDE increases the early Universe expansion rate which decreases the angular sound horizon and damping scales. These result in residual oscillations and a higher damping tail in the primary  $TT$  and  $TE$  spectra. The lack of significant deviations in the Planck CMB data for these modes, therefore, translates into upper limits on the allowed amount of EDE. Since the presence of EDE introduces increased Hubble friction at an early time, this enhanced friction suppresses the growth of density perturbations for modes with wave numbers  $k \gtrsim 0.01 \text{ hMpc}^{-1}$ , with the degree of suppression being contingent on the amount and duration of EDE. These modes, which enter the horizon around the time when the EDE contribution reaches its maximum, experience the strongest impact from the modified expansion rate [21]. These result in modifications to the matter power spectrum and hence show up in probes of structure growth that are

sensitive to the matter power spectrum in projection such as CMB lensing. These result in modifications to the matter power spectrum and hence show up in probes of structure growth that are sensitive to the matter power spectrum in projection such as CMB lensing. Previous analyses used Planck 2018 lensing measurements, but with the advent of new measurements from ACT data release 6 (DR6) and Planck PR4 with lower reconstruction noise, it is fitting to provide updated constraints on EDE. Furthermore, EDE analyses usually include BAO as a probe of the low-redshift expansion rate with data from Sloan Digital Sky Survey (SDSS), Baryon Oscillation Spectroscopic Survey (BOSS), and extended BOSS (eBOSS). BAOs provide independent constraints on  $\Omega_m$  to those from the CMB, which aid with degeneracy breaking when including extensions like EDE. It is therefore worthwhile to investigate whether the constraints are robust to the BAO dataset used. This motivates the analysis with new BAO measurements from DESI year 1 (DESI-Y1) data, which have similar constraining power as BOSS/eBOSS.

Bayesian inference involving EDE models can be time demanding: solving for the dynamics of the EDE field at a sufficiently high accuracy can take several minutes per step in a standard Markov chain Monte Carlo (MCMC) chain and a typical computing setup. Here we make use of neural network emulators constructed with CosmoPower [22], following the same strategy as in [23], to emulate the output of CLASS\_EDE [16].<sup>1</sup> We incorporate our EDE emulators into CLASS\_SZ [24] so they can easily be used in Bayesian analysis with the Cobaya sampler [25], which we use throughout. Our machine-learning-accelerated pipeline allows us to reach convergence within  $\mathcal{O}(10\text{h})$  instead of days or even weeks using full Boltzmann solutions. In all of our runs, we adopt a Gelman-Rubin convergence criterion with a threshold  $R - 1 < 0.01$ , compared to previous EDE analyses that used other thresholds, such as  $R - 1 < 0.05$  [26],  $R - 1 < 0.03$  [20], or  $R - 1 < 0.1$  [11]. While these differences in convergence criteria are unlikely to qualitatively alter the conclusions of previous studies, they may result in slightly different upper bounds. When directly comparing constraints across analyses, it is worth noting that less stringent convergence criteria can produce upper bounds that differ modestly from those obtained with stricter convergence requirements.

We perform extensive checks of emulator accuracy in Appendix C, reproducing existing results on relevant datasets.<sup>2</sup>

The priors adopted in this work are found in Appendix A. Unless otherwise stated we use three degenerate massive neutrino states, and when the neutrino mass is fixed we use  $\Sigma m_\nu = 0.06 \text{ eV}$  (with each neutrino carrying

<sup>1</sup>[https://github.com/mwt5345/class\\_ede](https://github.com/mwt5345/class_ede)

<sup>2</sup>See also [23,27] for further benchmarking and testing the emulators for current and futuristic datasets.

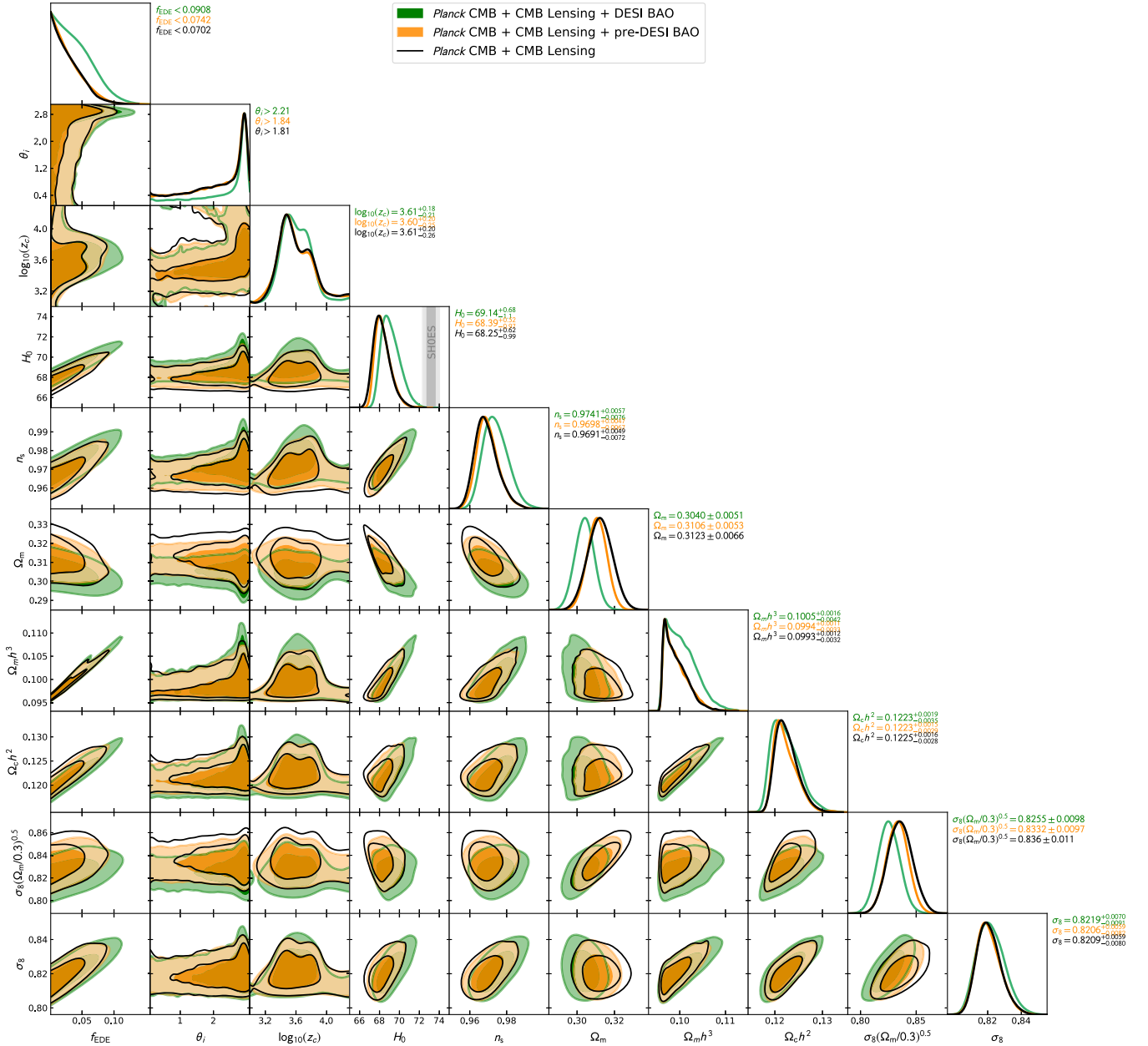


FIG. 1. Marginalized (1D and 2D) joint posterior probability distributions for the EDE parameters and a subset of other parameters in fits to our baseline Planck CMB + CMB lensing + DESI BAO data (green), Planck CMB + CMB lensing + pre-DESI BAO data (orange), and Planck CMB + CMB lensing only (black). The vertical gray bands in the  $H_0$  panel show the latest SH0ES constraint [2] as a reference.

0.02 eV). We keep the effective number of relativistic species at early times fixed to  $N_{\text{eff}} = 3.046$ . We work with a spatially flat  $\Lambda$ CDM(+EDE) cosmology throughout. We often refer to the derived parameters  $S_8 = \sigma_8(\Omega_m/0.3)^{0.5}$  and  $h = H_0/(100 \text{ km s}^{-1} \text{ Mpc}^{-1})$ .

## II. DATA AND LIKELIHOODS

In this analysis, we focus on CMB data and the improvements in constraints that the new DESI BAO and ACT DR6 CMB lensing data add. The datasets used are detailed below.

**Planck CMB:** We include temperature and polarization power spectra of the primary CMB as observed by the *Planck* satellite. Specifically, we use the small-scale  $\ell > 30$  TT, TE, and EE band powers analyzed from the Planck PR4 (NPIPE [28]) maps based on the Camspec likelihood [29]. We also include the Planck PR3 likelihood for the large-scale temperature power spectrum and large-scale polarization information that constrains the optical depth to reionization using the likelihood from the `SROLL` maps [30]. We will subsequently refer to the above combination as Planck CMB. We note that for one of our benchmark runs we also use Planck PR3 TTTEEE data, see Appendix C 4.

TABLE I. Marginalized constraints on key cosmological parameters in the EDE model (with power-law index  $n = 3$ ) in bold and other relevant cosmological parameters. Upper limits are given at the 95% confidence level (CL) while constraints are given at 68% CL.

Constraints on EDE ( $n = 3$ )						
Parameter	Planck CMB lensing DESI BAO	Planck CMB pre-DESI BAO	Planck CMB lensing	Planck CMB DESI BAO	Planck CMB	Planck 2018TT+TE + EE
$f_{\text{EDE}}$	$<0.091$	$<0.074$	$<0.070$	$<0.093$	$<0.081$	$<0.093$
$\log_{10}(z_c)$	$3.61^{+0.18}_{-0.21}$	$3.60^{+0.20}_{-0.25}$	$3.61^{+0.20}_{-0.26}$	$3.63^{+0.19}_{-0.22}$	$3.61^{+0.21}_{-0.24}$	$3.63 \pm 0.24$
$H_0$ (km/s/Mpc)	$69.14^{+0.68}_{-1.10}$	$68.39^{+0.52}_{-0.97}$	$68.25^{+0.62}_{-0.99}$	$69.19^{+0.66}_{-1.20}$	$68.37^{+0.68}_{-1.10}$	$68.42^{+0.79}_{-1.30}$
$\Omega_m$	$0.3027^{+0.0064}_{-0.0038}$	$0.3093^{+0.0066}_{-0.0038}$	$0.3109^{+0.0080}_{-0.0052}$	$0.3016^{+0.0067}_{-0.0040}$	$0.3106 \pm 0.0088$	$0.3146 \pm 0.0088$
$\Omega_c h^2$	$0.1223^{+0.0019}_{-0.0035}$	$0.1223^{+0.0015}_{-0.0029}$	$0.1225^{+0.0016}_{-0.0028}$	$0.1220^{+0.0019}_{-0.0038}$	$0.1228^{+0.0018}_{-0.0033}$	$0.1240^{+0.0021}_{-0.0041}$
$S_8$	$0.826 \pm 0.010$	$0.833 \pm 0.010$	$0.836 \pm 0.011$	$0.821 \pm 0.012$	$0.835 \pm 0.015$	$0.843 \pm 0.018$
$\sigma_8$	$0.822^{+0.007}_{-0.009}$	$0.821^{+0.006}_{-0.008}$	$0.821^{+0.006}_{-0.008}$	$0.818^{+0.009}_{-0.011}$	$0.821^{+0.008}_{-0.011}$	$0.823^{+0.010}_{-0.013}$
$R - 1$	0.006981	0.004575	0.009128	0.006200	0.009568	0.000990

CMB lensing: We employ CMB lensing power spectrum data from the ACT DR6 [31–33] and Planck PR4 (NPIPE) [28]. The ACT DR6 lensing map covers 9400 deg<sup>2</sup> and is signal dominated on scales  $L < 150$ , achieving a precision of 2.3% ( $43\sigma$ ). The Planck PR4 lensing analysis benefits from reprocessed maps with around 8% more data than PR3, resulting in a 20% increase in signal-to-noise ratio compared to the 2019 Planck PR3 release. We refer to the combined lensing likelihood from both experiments as our baseline, denoted as CMB lensing. We write “CMB lensing 2018” when we use the Planck 2018 CMB lensing likelihood [34].

DESI BAO: We consider BAO measurements from the DESI-Y1 release [35]. DESI measured BAO from the clustering of galaxies with samples spanning redshifts  $0.1 \leq z \leq 4.2$ . These include seven redshift bins comprising bright galaxy samples, luminous red galaxies (LRGs), emission line galaxies, quasars, and the Lyman- $\alpha$  forest sample. We use the official DESI likelihood, publicly available in Cobaya. In Appendix C 2 we show that we can recover the constraints in [35]. We denote the above as DESI BAO.

Pre-DESI BAO (and RSD): When specified, we also test data combinations that utilize BAO and redshift-space distortion (RSD) measurements from 6dFGS [36], the SDSS DR7 main galaxy sample [37], BOSS DR12 LRGs [38], and eBOSS DR16 LRGs [39], which we will subsequently denote as pre-DESI BAO (pre-DESI BAO and RSD when including growth information from RSD).

Pantheon+: In certain data combinations, we make use of SNIa from the Pantheon + compilation [40,41], which comprises 1550 spectroscopically confirmed SNIa in the redshift range  $0.001 \leq z \leq 2.26$ .

SHOES: This refers to the addition of SHOES Cepheid host distance anchors to Pantheon+ (see [41] for details). This is similar to adding a Gaussian prior on the peak SNIa

absolute magnitude,  $M_b$  as in [26], or a Gaussian prior on  $H_0$  as in, e.g., [20], but without approximation.

### III. RESULTS

#### A. New EDE constraints with Planck CMB + CMB lensing + DESI BAO

The baseline data combination adopted in this work with Planck CMB, new CMB lensing from ACT DR6 and Planck PR4 NPIPE, and new DESI BAO Y1 provides the following upper bound on EDE:

$$f_{\text{EDE}} < 0.091(0.0512) \quad 95\%(68\%) \text{ CL.} \quad (1)$$

The marginalized posterior probability distribution for this analysis is shown in Fig. 1 as the green contours. For the Hubble constant, we find

$$H_0 = 69.14^{+0.68}_{-1.1} \text{ km s}^{-1} \text{ Mpc}^{-1}. \quad (2)$$

This is in  $4.7\sigma$  tension with the latest SHOES-inferred value of  $73.17 \pm 0.86 \text{ km s}^{-1} \text{ Mpc}^{-1}$  [2] (see gray vertical band in the  $H_0$  panel of Fig. 1).

For completeness, we carry out the same analysis, substituting DESI BAO with pre-DESI BAO (orange contours in Fig. 1). In this case, we find a slightly tighter bound on EDE, namely,

$$f_{\text{EDE}} < 0.074(0.036) \quad 95\%(68\%) \text{ CL.} \quad (3)$$

The corresponding  $H_0$  constraint is

$$H_0 = 68.39^{+0.52}_{-0.97} \text{ km s}^{-1} \text{ Mpc}^{-1}, \quad (4)$$

in  $5.6\sigma$  tension with the latest SHOES-inferred value.

In Fig. 1, we also show the resulting constraints for the same analysis without BAO data in black.

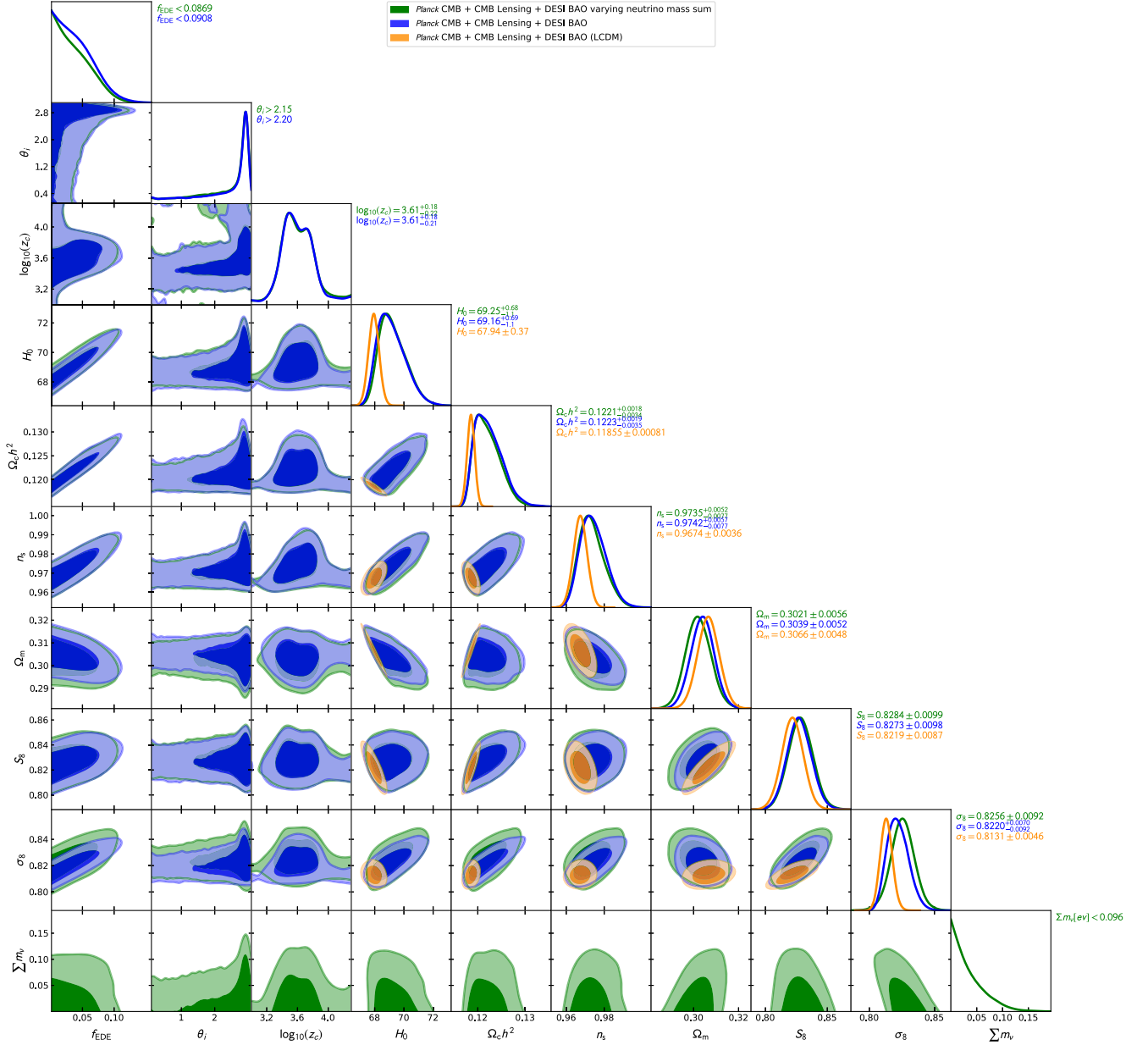


FIG. 2. Marginalized (1D and 2D) joint posterior probability distributions for the EDE parameters and a subset of other parameters in fits to our baseline Planck PR4 (NPIPE) TT + TE + EE data + ACT DR6 and PR4 CMB lensing + DESI BAO data (blue) compared to the analysis obtained with the same data combination but allowing the neutrino mass to vary (green). In orange we show the same dataset analyzed within  $\Lambda$ CDM.

This combination of Planck CMB and CMB lensing, i.e., ACT DR6 + Planck PR4 (NPIPE), yields our tightest EDE bound,

$$f_{\text{EDE}} < 0.070(0.036) \quad 95\%(68\%) \text{ CL.} \quad (5)$$

Comparing contours in Fig. 1, we see that the main effect of adding pre-DESI BAO to Planck CMB and CMB lensing is a tightening of the  $\Omega_m$  constraint. The effects on other parameters, including EDE parameters, are marginal.

Nonetheless, adding DESI BAO to Planck CMB and CMB lensing has an appreciable effect not only on  $\Omega_m$ <sup>3</sup> but also on  $n_s$ ,  $H_0$ , and  $f_{\text{EDE}}$ . The weakening of the upper bound on  $f_{\text{EDE}}$  (see top frame in triangle plot of Fig. 1) can be attributed to the fact that DESI BAO data are pushing the model toward a matter fraction that is  $1.2\sigma$  lower than the  $\Omega_m$

<sup>3</sup>We note that the constraining power of pre-DESI and DESI BAO on  $\Omega_m$  is nearly the same, but DESI BAO prefers a lower  $\Omega_m$ .

TABLE II. Marginalized constraints on key cosmological parameters in the EDE model (with power-law index  $n = 3$ ). EDE parameters are in bold. Upper limits are given at the 95% CL while constraints are given in 68% CL. The first two columns of the first row show constraints obtained with a data combination that matches that of [26]. We then explore the effects of including new DESI BAO and CMB lensing from ACT DR6 and Planck PR4 (NPIPE).

Constraints on EDE ( $n = 3$ )					
Parameter	CMB (low- $\ell$ EE 2018)	CMB (low- $\ell$ EE 2018)	CMB (low- $\ell$ EE 2018)	CMB (low- $\ell$ EE 2018)	CMB (low- $\ell$ EE 2018)
	CMB lensing 2018 pre-DESI BAO + RSD Pantheon+	CMB lensing 2018 pre-DESI BAO + RSD Pantheon + SH0ES $M_b$ prior	CMB lensing 2018 pre-DESI BAO + RSD Pantheon + SH0ES $M_b$ prior	CMB lensing 2018 pre-DESI BAO + RSD Pantheon + SH0ES $M_b$ prior	CMB lensing 2018 pre-DESI BAO + RSD Pantheon + SH0ES $M_b$ prior
$f_{\text{EDE}}$	$< 0.070$	$0.110 \pm 0.023$	$0.110 \pm 0.023$	$< 0.087$	$0.114 \pm 0.023$
$\log_{10}(z_c)$	$3.60^{+0.23}_{-0.26}$	$3.64^{+0.17}_{-0.19}$	$3.64^{+0.17}_{-0.19}$	$3.61^{+0.20}_{-0.23}$	$3.64 \pm 0.11$
$H_0$ (km/s/Mpc)	$68.14^{+0.50}_{-0.92}$	$71.20 \pm 0.79$	$71.20 \pm 0.79$	$68.83^{+0.60}_{-1.1}$	$71.69 \pm 0.80$
$\Omega_m$	$0.3130 \pm 0.0052$	$0.3031 \pm 0.0050$	$0.3031 \pm 0.0050$	$0.3067 \pm 0.0051$	$0.2980 \pm 0.0046$
$\Omega_c h^2$	$0.1224^{+0.0013}_{-0.0029}$	$0.1304 \pm 0.0030$	$0.1304 \pm 0.0030$	$0.1223^{+0.0017}_{-0.0035}$	$0.1299 \pm 0.0029$
$S_8$	$0.834 \pm 0.011$	$0.842 \pm 0.012$	$0.842 \pm 0.012$	$0.827 \pm 0.011$	$0.835 \pm 0.011$
$\sigma_8$	$0.8165^{+0.0070}_{-0.0091}$	$0.8375 \pm 0.0092$	$0.8375 \pm 0.0092$	$0.8179^{+0.0080}_{-0.010}$	$0.8378 \pm 0.0091$
$R - 1$	0.00283	0.00866	0.00866	0.00306	0.00674
Parameter	CMB (low- $\ell$ EE 2018)	CMB (low- $\ell$ EE 2018)	CMB (low- $\ell$ EE 2018)	CMB (low- $\ell$ EE 2018)	CMB (low- $\ell$ EE 2018)
	CMB lensing pre-DESI BAO + RSD Pantheon+	CMB lensing pre-DESI BAO + RSD Pantheon + SH0ES $M_b$ prior	CMB lensing pre-DESI BAO + RSD Pantheon + SH0ES $M_b$ prior	CMB lensing pre-DESI BAO + RSD Pantheon + SH0ES $M_b$ prior	CMB lensing pre-DESI BAO + RSD Pantheon + SH0ES $M_b$ prior
$f_{\text{EDE}}$	$< 0.073$	$0.108 \pm 0.023$	$0.108 \pm 0.023$	$< 0.080$	$0.114 \pm 0.022$
$\log_{10}(z_c)$	$3.60^{+0.21}_{-0.26}$	$3.63^{+0.15}_{-0.18}$	$3.63^{+0.15}_{-0.18}$	$3.59^{+0.19}_{-0.21}$	$3.63 \pm 0.11$
$H_0$ (km/s/Mpc)	$68.23^{+0.54}_{-0.93}$	$71.18 \pm 0.78$	$71.18 \pm 0.78$	$68.13^{+0.48}_{-0.86}$	$71.73 \pm 0.80$
$\Omega_m$	$0.3115^{+0.0065}_{-0.0037}$	$0.3025 \pm 0.0049$	$0.3025 \pm 0.0049$	$0.3055^{+0.0063}_{-0.0037}$	$0.2974 \pm 0.0045$
$\Omega_c h^2$	$0.1227^{+0.0015}_{-0.0030}$	$0.1300 \pm 0.0028$	$0.1300 \pm 0.0028$	$0.1224^{+0.0018}_{-0.0034}$	$0.1297^{+0.0027}_{-0.0030}$
$S_8$	$0.8336 \pm 0.0098$	$0.840 \pm 0.011$	$0.840 \pm 0.011$	$0.8268 \pm 0.0096$	$0.834 \pm 0.010$
$\sigma_8$	$0.8181^{+0.0065}_{-0.0082}$	$0.8363 \pm 0.0077$	$0.8363 \pm 0.0077$	$0.8194^{+0.0071}_{-0.0089}$	$0.8374 \pm 0.0080$
$R - 1$	0.00960	0.00918	0.00918	0.00697	0.00566

value preferred by pre-DESI BAO and CMB data. Indeed, the combination of CMB and BAO data leads to a negative degeneracy between  $\Omega_m$  and  $H_0$ , as well as  $\Omega_m$  and  $n_s$ , while both  $H_0$  and  $n_s$  have a positive degeneracy with  $f_{\text{EDE}}$ .

In Table I we report constraints on a relevant subset of parameters for the analyses of Fig. 1, as well as for other combinations of datasets: without lensing, with Planck CMB only (i.e., PR4) and with Planck 2018 CMB (i.e., PR3). We find that switching from Planck PR3 to Planck PR4 CMB yields a  $\approx 10\%$  more constraining bound on  $f_{\text{EDE}}$ . As discussed above, adding DESI BAO slightly degrades the bound because of the lower  $\Omega_m$ . Moreover, comparing the results in the third and fifth column show that adding CMB lensing tightens the bound on  $f_{\text{EDE}}$  by another  $\approx 10\%$ . Marginalized posterior probability distributions for all analyses in Table I (except the last column with Planck 2018) are shown in Fig. 4 in Appendix B.

Making use of our Boltzmann code emulators, we can study further extensions to the  $\Lambda$ CDM model. In particular, we can investigate the stability of the neutrino mass bound obtained in [35] in cosmological models with EDE. Using our baseline dataset (Planck CMB + CMB lensing + DESI BAO), we consider a model with EDE and massive neutrinos, with the neutrino mass sum as a free parameter. The contours are shown in green in Fig. 2 together with the fixed neutrino mass analysis (blue contours) and  $\Lambda$ CDM as a reference in orange. In agreement with [42], we find no statistically significant degeneracies between the EDE parameter space and  $\sum m_\nu$ . The addition of free neutrino mass does not change the constraint on  $f_{\text{EDE}}$  in a substantial way. Conversely, adding EDE changes the neutrino mass bound by only a small amount, going from  $\sum m_\nu < 0.072$  eV (95%CL) in  $\Lambda$ CDM [35] to  $\sum m_\nu < 0.097$  eV (95%CL).

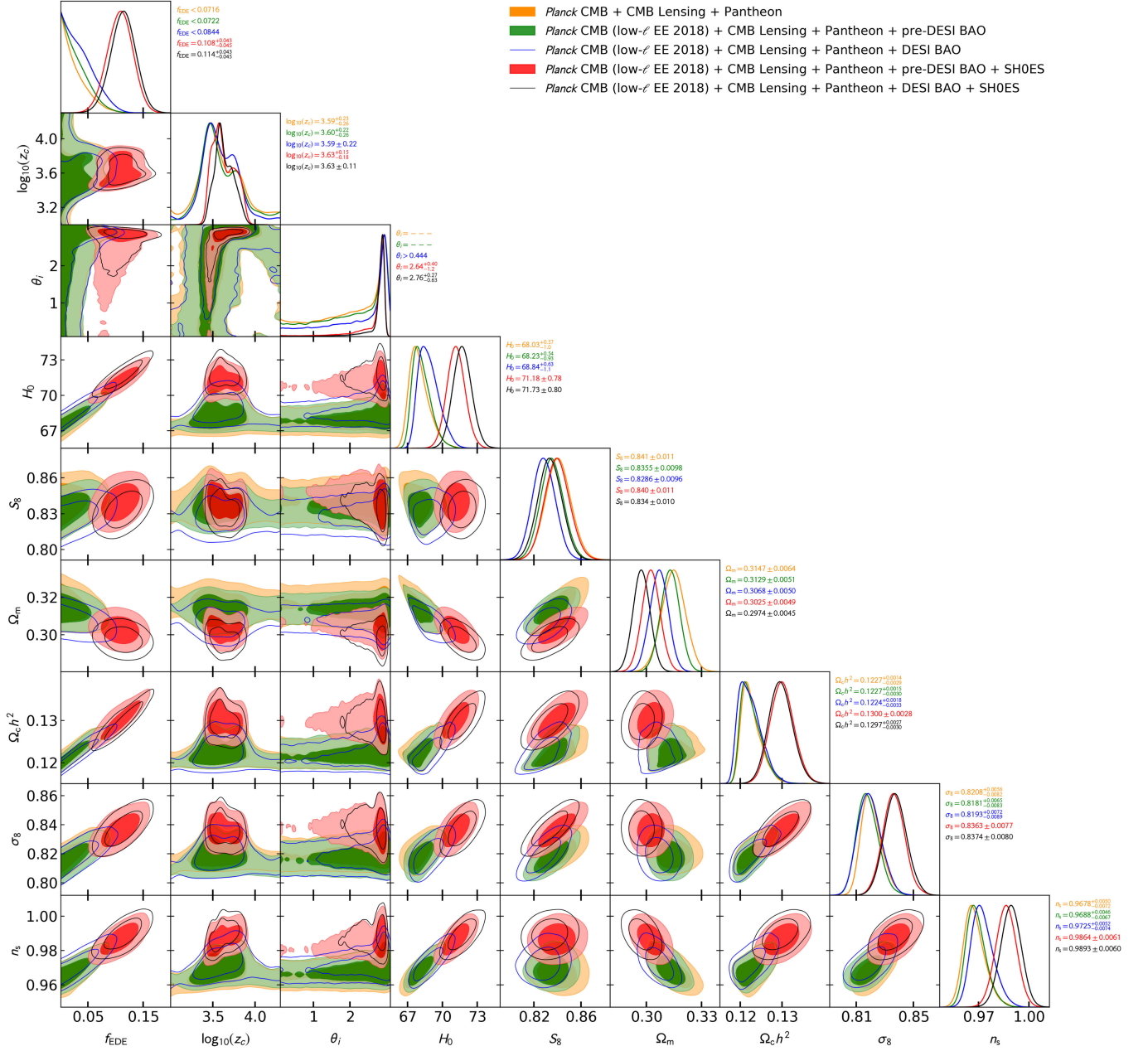


FIG. 3. Marginalized (1D and 2D) joint posterior probability distributions for the EDE parameters and a subset of other cosmological parameters of interest in analyses that include the Pantheon + type Ia supernova dataset, with and without SH0ES Cepheid host distance anchors. See Sec. III B for details.

Given that EDE parameters and  $\sum m_\nu$  do not have statistically significant degeneracies, we only report results keeping the neutrino mass sum fixed to the minimum value allowed by the normal hierarchy of  $\sum m_\nu = 0.06$  eV in the remainder of this paper.

## B. Inclusion of Pantheon + SNIa

In [26], upper bounds on  $f_{\text{EDE}}$  were provided using a combination of Planck PR4 (NPIPE) TT/TE/EE, low- $\ell$ TT

and EE likelihoods<sup>4</sup> from Planck 2018, Planck 2018 CMB lensing, measurements of the BAO and RSD from the CMASS and LOWZ galaxy samples of BOSS DR12, 6dFGS, and SDSS DR7, and the Pantheon + catalog of over 1600 SNIa.

<sup>4</sup>The CMB primary combination used here is similar to that of our baseline analysis, with the exception of the low- $\ell$ EE data, where we use a more updated version based on Sroll; we will thus denote this CMB primary combination as CMB (low- $\ell$ EE 2018).

For the same data combination, but setting a more stringent convergence criterion of  $R - 1 < 0.01$  (compared to the  $R - 1 < 0.05$  of [26]), we find

$$f_{\text{EDE}} < 0.070(95\% \text{ CL}), \quad h = 0.6814_{-0.0092}^{+0.0050}(68\% \text{ CL}). \quad (6)$$

(See the first column at the top of Table II for details.) This is consistent with the results from [26], namely,

$$f_{\text{EDE}} < 0.061(95\% \text{ CL}) \quad h = 0.6811_{-0.0082}^{+0.0048}(68\% \text{ CL}). \quad (7)$$

Furthermore, we consider the addition of the SH0ES Cepheid host distances to Pantheon+, similar to the Gaussian prior on  $M_b$  used in [26], but without approximation.

Our results are in the second column at the top of Table II. We find

$$f_{\text{EDE}} = 0.110 \pm 0.023(68\% \text{ CL}), \quad (8)$$

$$h = 0.7120 \pm 0.0079(68\% \text{ CL}), \quad (9)$$

consistent with the results from [26], namely,

$$f_{\text{EDE}} = 0.107 \pm 0.023(68\% \text{ CL}), \quad (10)$$

$$h = 0.7124 \pm 0.0077(68\% \text{ CL}). \quad (11)$$

The small differences between our results and those of [26] can be attributed to a combination of the different convergence of the chains<sup>5</sup> and possibly different implementations of the EDE model.<sup>6</sup>

In Table II, we provide updated versions of these bounds using the same dataset but replacing the CMB lensing and BAO data with the new ACT DR6 and Planck PR4 (NPIPE) CMB lensing measurement and DESI BAO data. In Fig. 3, we show the marginalized posterior probability distributions for the updated constraints. We also plot the contours (orange) for an analysis without BAO but including Pantheon+ (as well as CMB and CMB lensing), yielding  $f_{\text{EDE}} < 0.0716$  (95% CL). Similar to the previous section, we find that the tightest bound on EDE is achieved in the analysis without BAO.

#### IV. DISCUSSION AND CONCLUSION

We provide updated constraints on axionlike EDE in light of new BAO data from DESI Y1 and CMB lensing measurements from ACT DR6 and Planck PR4.

Our main results are summarized in Tables I and II. We find that, using CMB and CMB lensing alone, one can

<sup>5</sup>By truncating the initial and final parts of our converged chains, we checked that larger  $R - 1$  values are associated with more variance in the estimated bounds, typically 10% for  $R - 1 \approx 0.05$ .

<sup>6</sup>We use the public CLASS\_EDE code [16], while [26] refers to a different modified version of CLASS.

place strong constraints on the maximum fractional contribution of EDE to the total energy density, with  $f_{\text{EDE}} < 0.070(95\%)$ . The addition of DESI slightly degrades this bound to  $f_{\text{EDE}} < 0.091(95\% \text{ CL})$  due to the low value of  $\Omega_m$  preferred by DESI. Nevertheless, the data do not show any statistically significant preference for EDE. This is shown in the black open contour of our main plot in Fig. 1. As a guide, it is pointed out in [11,15,20] that a  $f_{\text{EDE}} = 0.1$  at a redshift  $z_c$  around matter-radiation equality is required for EDE to be a viable model in resolving the Hubble tension.

The lack of EDE preference is confirmed by comparing  $\chi^2$  values of the various experiments for  $\Lambda\text{CDM}$  to those from EDE, as shown in Tables III and IV. When adding the three additional EDE parameters, there is a total  $\Delta\chi^2 \equiv \chi_{\text{EDE}}^2 - \chi_{\Lambda\text{CDM}}^2 = -1.07$  (including Camspec NPIPE, CMB lensing, and DESI BAO), which is not statistically significant. Moreover, by comparing the rightmost two columns of Table IV, when using the EDE model with Pantheon+, adding a SH0ES prior increases the  $\chi^2$  of the fit to Camspec NPIPE by 4.9 as compared with a run that does not include the SH0ES prior. For a model to successfully resolve the Hubble tension, it must not worsen the fit to Planck when imposing the SH0ES prior. (See also the discussion in [26] regarding alternative methods that use profile likelihoods to assess whether a model can address the Hubble tension.)

When using pre-DESI BAO that prefers a slightly higher  $\Omega_m$  instead of DESI BAO, the EDE bounds tighten again to  $f_{\text{EDE}} < 0.074(95\% \text{ CL})$ . One of the main qualitative conclusions of this work is that the constraints on EDE are robust to the BAO dataset used, and inclusion of BAO does not tighten the constraints on EDE parameters significantly compared to what CMB and CMB lensing already achieve.

Previous work has shown EDE cosmologies are inconsistent with the Lyman- $\alpha$  forest, yielding  $> 4\sigma$  tension with SH0ES and placing constraints on EDE such that  $f_{\text{EDE}} < 0.03(95\% \text{ CL})$  [43]. Unlike [19,20,44,45], we do not find any hint for nonzero EDE using CMB and BAO data. In [20], the combination of ACT DR4 high- $\ell$ TT/TE/EE [46,47] with Planck 2018 low- $\ell$  and Planck 2018 CMB lensing and pre-DESI BAO gave an  $\approx 3\sigma$  hint of EDE, with  $f_{\text{EDE}} = 0.091_{-0.036}^{+0.020}$  (68% CL), while our baseline constraints using

TABLE III. Best fit  $\chi^2$  for each experiment and the total  $\chi_{\text{total}}^2$ . These values are reported for the  $\Lambda\text{CDM}$  and EDE models with our baseline dataset. The  $\Delta\chi^2$  values for the  $\Lambda\text{CDM}$  and EDE models are also shown.

	$\Lambda\text{CDM}$	EDE	$\Delta\chi^2 = \chi_{\text{EDE}}^2 - \chi_{\Lambda\text{CDM}}^2$
Camspec NPIPE	10542.61	10542.60	-0.01
TTTEEE			
CMB lensing	19.81	20.38	0.57
DESI BAO	15.64	14.01	-1.63
$\chi_{\text{total}}^2$	10578.06	10576.99	-1.07

TABLE IV. Best fit  $\chi^2$  for each experiment, the total  $\chi_{\text{total}}^2$ , and  $\chi_{\text{com}}^2$  which consists of the subset of experiments common to all the combinations reported, specifically Camspec NPIPE TTTEEE, CMB lensing, and DESI BAO. These values are reported for the  $\Lambda$ CDM and EDE models with our baseline dataset. Furthermore,  $\chi_{\text{com,noDESI}}^2$  is the same as  $\chi_{\text{com}}^2$  but excludes DESI BAO.

	$\Lambda$ CDM	EDE	EDE with Pantheon+	EDE with Pantheon+ +SHOES prior
Camspec NPIPE TTTEEE	10542.6	10542.6	10541.1	10546.0
CMB lensing	19.8	20.4	20.6	21.0
DESI BAO	15.6	14.0	14.9	12.8
Pantheon+	...	...	1405.3	1460.5
$\chi_{\text{total}}^2$	10578.0	10577.0	11981.9	12040.3
$\chi_{\text{com}}^2$	10578.0	10577.0	10576.6	10579.8
$\chi_{\text{com,no DESI}}^2$	10562.4	10563.0	10561.7	10567.0

Planck CMB NPIPE + ACT DR6 + Planck PR4 CMB lensing and DESI BAO give an upper bound of  $f_{\text{EDE}} < 0.091$  (95% CL). Whether or not the mild preference of ACT DR4 for a nonzero  $f_{\text{EDE}}$  is a subtle systematic artifact or a sign for new physics will likely be elucidated with the upcoming ACT DR6 and SPT-3G [48] CMB power spectra measurements.

An important note is that MCMC chain convergence must be handled carefully, as a lack of true convergence can produce artificially tight bounds on parameters. In this work, we have imposed more stringent convergence criteria, requiring a Gelman-Rubin threshold of  $R - 1 < 0.01$  for convergence compared with the  $R - 1 < 0.05$  [26] and  $R - 1 < 0.03$  [20] used in previous works.

Furthermore, our analysis demonstrates the capability of accelerated inference with neural network emulators to efficiently explore parameter spaces and derive robust constraints within a reasonable time frame. Without emulators, the work presented here could not have been carried out within only a few weeks from the release of the DESI BAO data.

Previous work has investigated the use of a profile likelihood to mitigate prior-volume effects that may bias Bayesian inference in the EDE context [26,49] (though such effects were found to be minimal in [26]). We note that emulators may complicate the convergence of a profile likelihood due to small numerical noise in the emulator outputs. Additionally, since the  $\Delta\chi^2$  between the baseline  $\Lambda$ CDM and EDE models is only  $\approx 1$  for three additional parameters, and since the Bayesian posteriors do not suggest preference for the EDE model, we find no preference for the EDE model in either the Bayesian or frequentist framework. Therefore, we do not find it necessary to perform a profile likelihood here given the high computational cost. We thus leave the investigation into the use of emulators with a profile likelihood to future work using tools such as those described in [50,51].

We acknowledge the use of GetDist [52] for analyzing and plotting MCMC results.

## ACKNOWLEDGMENTS

We are indebted to Antony Lewis for providing the relevant DESI and Pantheon+ likelihood files in Cobaya and for helpful discussions. We are also grateful to Erminia Calabrese, Mathew Madhavacheril, Emmanuel Schaan, Alessio Spurio-Mancini, Arthur Kosowsky, Julien Lesgourgues, and George Efstathiou for discussions. We thank Nick Carriero, Robert Blackwell, and Dylan Simon from the Flatiron Institute for key computational advice. F.J.Q. and B.D.S. acknowledge support from the European Research Council (ERC) under the European Union’s Horizon 2020 research and innovation program (Grant Agreement No. 851274). B.D.S. further acknowledges support from an STFC Ernest Rutherford Fellowship. K.M.S. acknowledges support from the National Science Foundation Graduate Research Fellowship Program under Grant No. DGE 2036197. J.C.H. acknowledges support from NSF Grant No. AST-2108536, DOE Grant No. DE-SC0011941, NASA Grants No. 21-ATP21-0129 and No. 22-ADAP22-0145, the Sloan Foundation, and the Simons Foundation. Computations were performed on the Niagara supercomputer at the SciNet HPC Consortium. SciNet is funded by Innovation, Science and Economic Development Canada; the Digital Research Alliance of Canada; the Ontario Research Fund: Research Excellence; and the University of Toronto. We acknowledge the use of computational resources at the Flatiron Institute. The Flatiron Institute is supported by the Simons Foundation. We also acknowledge the use of computational resources from Columbia University’s Shared Research Computing Facility project, which is supported by NIH Research Facility Improvement Grant No. 1G20RR030893-01, and associated funds from the New York State Empire State Development, Division of Science Technology and Innovation (NYSTAR) Contract No. C090171, both awarded April 15, 2010.

## APPENDIX A: PRIORS USED

We sample the parameter space spanned by  $\{f_{\text{EDE}}, \log_{10}(z_c), \theta_i, \ln(10^{10}A_s), H_0, n_s, \Omega_b h^2, \Omega_c h^2, \tau\}$ . As pointed out in [19,20], the choice of prior range for  $\log_{10}(z_c)$  is important because if it is extended to arbitrarily high redshifts, the parameter space is opened up, enabling  $f_{\text{EDE}}$  to take large values without having an impact on the CMB or other observables. Table V shows the priors used in this work. For the cases where we vary the neutrino mass sum, we adopt a broad uninformative uniform prior of  $\sum m_\nu$  of [0,5] eV.

TABLE V. Priors used in the EDE cosmological analysis of this work. Uniform priors are shown in square brackets and Gaussian priors with mean  $\mu$  and standard deviation  $\sigma$  are denoted  $\mathcal{N}(\mu, \sigma)$ .

Parameter	Prior
$f_{\text{EDE}}$	[0.001, 0.5]
$\log_{10}(z_c)$	[3,4.3]
$\theta_i$	[0.1, 3.1]
$\ln(10^{10}A_s)$	[2.5, 3.5]
$H_0$	[50, 90]
$n_s$	[0.8, 1.2]
$\Omega_b h^2$	$\mathcal{N}(0.02233, 0.00036)$
$\Omega_c h^2$	[0.005, 0.99]
$\tau$	[0.01, 0.8]

## APPENDIX B: FULL MARGINALIZED POSTERIOR PLOTS OF DIFFERENT DATASET COMBINATIONS

We show in Fig. 4 the full marginalized posteriors of the different subsets of the datasets used in the main analysis. For visualization purposes, we also show 95%CL bands centered at the mean value of the latest SH0ES, TRGB, and Planck measurements. None of the data combinations used are enough to bring the value of  $H_0$  up to fully resolve the Hubble tension.

## APPENDIX C: ROBUSTNESS TESTS

### 1. Emulators for EDE

Our emulators are constructed with CosmoPower [22], a wrapper for TensorFlow optimized for cosmological applications (see [53] for similar work in Julia). The architecture of the neural networks and details on how they are produced can be found in [22,23]. The emulators for CMB spectra and distances were trained on 196091 samples spread in a Latin hypercube spanning the parameter space (with a test-train split of 80%). The input layer of the neural network emulators is the set of six  $\Lambda$ CDM parameters, namely,  $A_s, n_s, \tau_{\text{reio}}, \Omega_c h^2, \Omega_b h^2$ , and  $H_0$  supplemented by the neutrino mass, the number of effective relativistic degrees of freedom in the early Universe  $N_{\text{eff}}$ , and the tensor-to-scalar ratio  $r$ . The generation of training data was done using a version of the Boltzmann code CLASS [54,55] adapted to EDE models, CLASS\_EDE<sup>7</sup> [16]. We used the version of the code corresponding to the commit of February 16, 2023 on the GitHub repository,<sup>8</sup> which is based on version v2.8.2 of CLASS. We note that this CLASS version could not allow extremely high-accuracy computation of the CMB high- $\ell$  regime because of its treatment of the Limber approximation for lensing. Hence, our current emulators will likely be obsolete in the stage IV era. Nonetheless, as shown hereafter, the accuracy of our emulators is sufficient for the data analysis carried out in this paper. The precision settings adopted for the generation of the training data are as follows:

- (i) perturb\_sampling\_stepsize: 0.05;
- (ii) neglect\_CMB\_sources\_below\_visibility: 1e-30;
- (iii) transfer\_neglect\_late\_source: 3000;
- (iv) halofit\_k\_per\_decade: 3000;
- (v) accurate\_lensing: 1;
- (vi) num\_mu\_minus\_lmax: 1000;
- (vii) delta\_l\_max: 1000;
- (viii) k\_min\_tau0: 0.002;
- (ix) k\_max\_tau0\_over\_l\_max: 3;
- (x) k\_step\_sub: 0.015;
- (xi) k\_step\_super: 0.0001;
- (xii) k\_step\_super\_reduction: 0.1;
- (xiii) P\_k\_max\_h/Mpc: 55/h;
- (xiv) l\_max\_scalars: 11000.

<sup>7</sup>[https://github.com/mwt5345/class\\_ede](https://github.com/mwt5345/class_ede)

<sup>8</sup>[https://github.com/mwt5345/class\\_ede/commit/199fbab08a5545c9f478c8137a1348c824d4874f](https://github.com/mwt5345/class_ede/commit/199fbab08a5545c9f478c8137a1348c824d4874f)

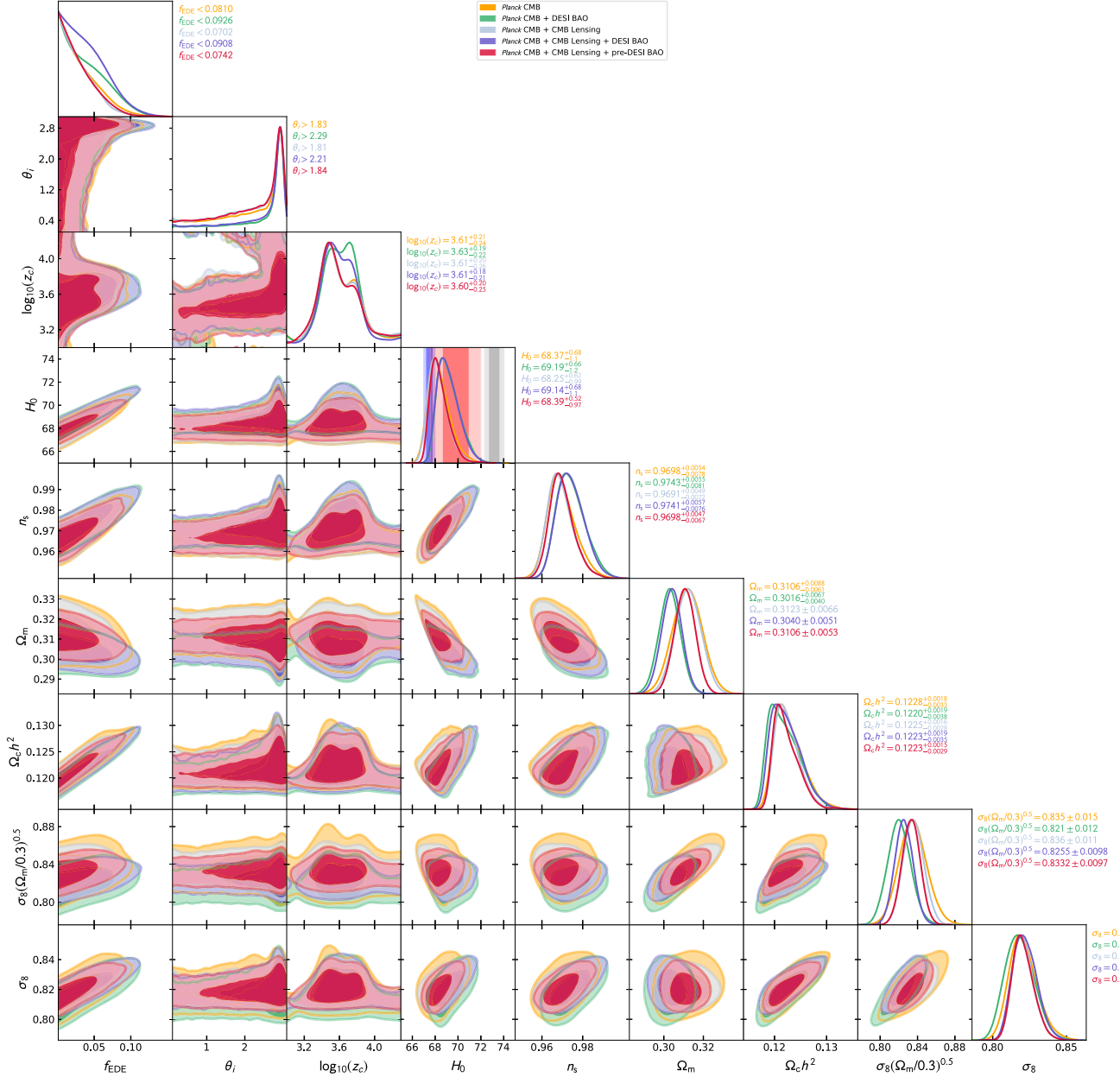


FIG. 4. Marginalized (1D and 2D) joint posterior probability distributions for the EDE parameters and a subset of other cosmological parameters of interest in fits to our baseline Planck PR4 (NPIPE) TT + TE + EE data + ACT DR6 and PR4 CMB lensing + DESI BAO data (blue). The vertical gray/magenta/blue bands in the  $H_0$  panel show the latest SH0ES [40], TRGB, [5] and Planck constraints, respectively. See Table I for a summary of these constraints and Sec. III A for discussion.

These settings are the same as in [20] except that we do not set `l_switch_limber=40` but `perturb_sampling_stepsize` as indicated instead. The other difference is that we use  $55/h$  rather than  $100$  for  $\mathcal{P}_k$  max  $h/\text{Mpc}$ . These settings are motivated by the accuracy settings investigations carried out in [20,23,56].

The CMB temperature and polarization spectra, and lensing potential power spectra, cover the multipole  $2 \leq \ell \leq 11,000$ . Along with these, three redshift-dependent quantities are emulated over a redshift range  $0 < z < 20$ ,

namely, the Hubble parameter  $H(z)$ , the angular diameter distance  $D_A(z)$ , and the root-mean-square of the matter overdensity field smoothed over a spherical region of radius  $8 \text{ Mpc}$ ,  $\sigma_8(z)$ . These redshift-dependent quantities constitute the building blocks for the theoretical prediction of BAO distance and RSD measurements. We also record and emulate a set of 16 derived parameters such as  $\sigma_8$  (at  $z=0$ ) or the primordial helium fraction. Our recombination and big bang nucleosynthesis models correspond to the current fiducial settings of CLASS\_EDE: RECFAST [57–59] and

Parthenope [60] with a fiducial  $N_{\text{eff}} = 3.046$  using v1.2 of the code for a neutron lifetime of 880.2 s, identical to standard assumptions of Planck 2017 papers, respectively. Nonlinear matter clustering is modeled with HMCODE following implementation from [61] and with  $\Lambda$ CDM-only prescription, i.e.,  $\eta_0 = 0.603$  and  $c_{\text{min}} = 3.13$  (following CLASS notations).

## 2. DESI BAO likelihood

To test the likelihood, we reproduce benchmark constraints from [35]. We use the latest DESI BAO data [35] and its associated likelihood publicly available in the MCMC sampler *Cobaya* package [62]. This likelihood should correspond exactly to the one used in [35]. To confirm this, we reproduce the constraints in the first line of Table 4 of [35], with DESI Y1 BAO data in combination with CMB. The CMB data are made of `planck_2018_lowl.TT`, `planck_2018_lowl.EE_scroll2`, and `planck_NPIPE_highl_CamSpec.TTTEEE`, as well as CMB lensing from ACT DR6 and NPIPE (without the inclusion of the normalization correction<sup>9</sup>). The BAO data correspond to the baseline, i.e., our DESI BAO (see main text). In [35], these data are analyzed within  $\Lambda$ CDM with three degenerate massive neutrinos and  $N_{\text{eff}} = 3.044$ , finding

$$\begin{aligned}\Omega_m &= 0.3037 \pm 0.0053 (68\% \text{ CL}), \\ h &= 0.6827 \pm 0.0042 (68\% \text{ CL}), \\ \Sigma m_\nu &< 0.072 \text{ eV} (95\% \text{ CL}).\end{aligned}\quad (\text{C1})$$

First, we analyze these data with the  $\Lambda$ CDM emulator from [23] with three degenerate massive neutrinos and  $N_{\text{eff}} = 3.046$ . We find

$$\begin{aligned}\Omega_m &= 0.3037 \pm 0.0050 (68\% \text{ CL}), \\ h &= 0.6817 \pm 0.0040 (68\% \text{ CL}), \\ \Sigma m_\nu &< 0.0735 \text{ eV} (95\% \text{ CL}).\end{aligned}\quad (\text{C2})$$

Thus, our result is  $0.24\sigma$  below the [35] result for  $h$ , and we obtain a  $\approx 2\%$  lower value for the 95% CL upper limit on  $\Sigma m_\nu$ . We recover their value for  $\Omega_m$  to exact precision. This shows that the DESI likelihood we are using in this work is fully consistent with the one used in the official DESI paper.

In a second step, we analyze the same data combination with the EDE emulators, but setting the lowest possible amount of EDE, namely,  $f_{\text{EDE}} = 0.001$  (`CLASS_EDE` does not allow for a lower value of  $f_{\text{EDE}}$ ) and the other EDE parameters set to  $\log_{10} z_c = 3.72$  and  $\theta_{i,\text{scf}} = 2.97$ . These values for  $z_c$  and  $\theta_{i,\text{scf}}$  are the best fit values from Table II of [20]. We find

<sup>9</sup>DESI Y1 analysis used a version of the DR6 lensing likelihood release where this correction is effectively not applied, although the effect of applying versus not applying is very small for cosmological parameters of interest.

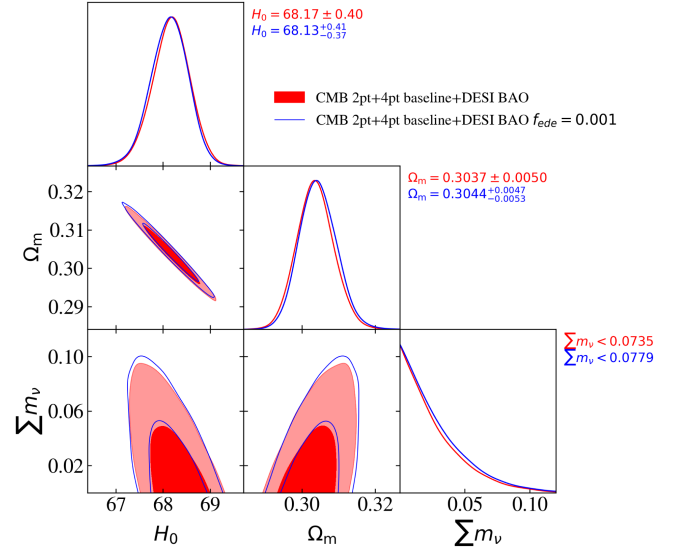


FIG. 5. Marginalized (1D and 2D) joint posterior probability distributions for  $\Sigma m_\nu$ ,  $H_0$ , and  $\Omega_m$  from the combination of CMB primary, CMB lensing, and DESI BAO with  $f_{\text{EDE}} = 0.001$ . See text for details.

$$\begin{aligned}\Omega_m &= 0.3044^{+0.0047}_{-0.0053} (68\% \text{ CL}), \\ h &= 0.6813^{+0.0041}_{-0.0037} (68\% \text{ CL}), \\ \Sigma m_\nu &< 0.0779 \text{ eV} (95\% \text{ CL}).\end{aligned}\quad (\text{C3})$$

Thus, these EDE emulator results are  $0.14\sigma$  above and  $0.1\sigma$  below the non-EDE emulator results (from the previous paragraph) for  $\Omega_m$  and  $h$ , respectively. The 95% CL neutrino mass sum limit also increases by  $\approx 6\%$ . These differences are likely explained by the fact that there is still a small amount of EDE. However, again, the differences are a small fraction of the uncertainties, which shows that our EDE emulators are suited for analyzing current DESI BAO data without any statistically significant bias.

Contours for both analyses described here are shown in Fig. 5.

## 3. ACT DR4 TTTEEE EDE constraints benchmark

To validate our emulators at the level of CMB temperature and polarization spectra, we reproduce EDE constraints from [20]. We use the public, foreground marginalized, likelihood code `PYACTLIKE`.<sup>10</sup> The data are stored in the same online repository and presented in detail in [46,47]. We reproduce results corresponding to the last two columns of Table II of [20], which use ACT DR4 TT + TE + EE spectra along with a Gaussian prior on the optical depth  $\tau = 0.065 \pm 0.015$  (mean and standard deviation). Although these results were obtained with the same EDE code, `CLASS_EDE`, there are minor differences between our emulator settings and the settings of [20]. In addition to

<sup>10</sup><https://github.com/ACTCollaboration/pyactlike>

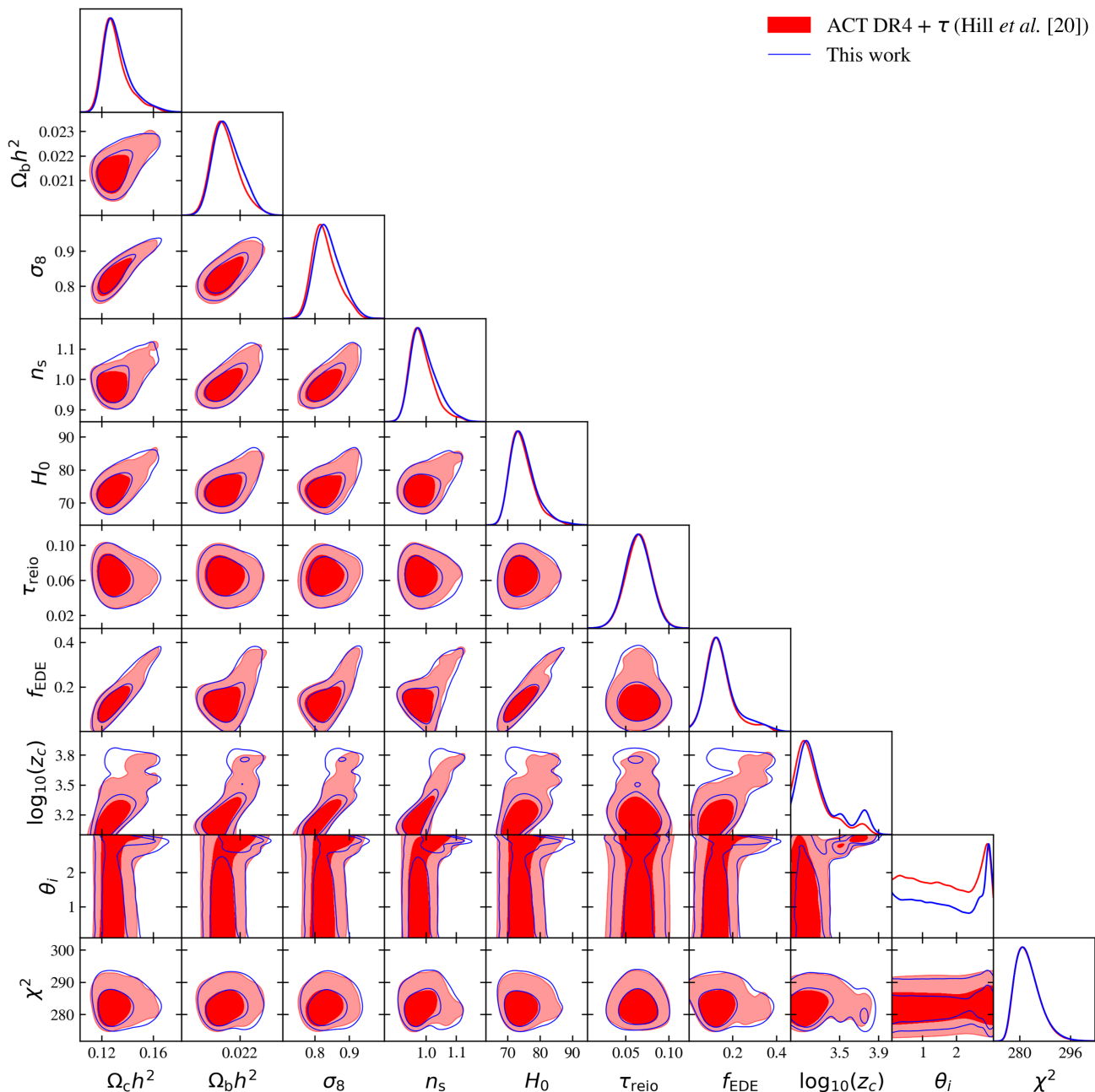


FIG. 6. Marginalized (1D and 2D) joint posterior probability distributions of EDE parameters and a subset of other parameters in fits of ACT DR4 CMB data in combination with a Gaussian prior on the optical depth. See text for details.

slightly different precision settings (see above), for the nonlinear evolution we use HMCODE, while [20] used HALOFIT, and for neutrinos, we use three degenerate massive neutrinos, while [20] used one massive and two massless neutrinos. Furthermore, [20] required a convergence criterion of  $R - 1 < 0.03$ , while we require at least  $R - 1 < 0.01$ . By reanalyzing the chains from [20] (publicly available online<sup>11</sup>), excluding 10% of burn-in, we get a

convergence criterion of  $R - 1 = 0.0117$ . In comparison, our chains have  $R - 1 = 0.0023$  (excluding 20% of burn-in).

As shown in Fig. 6, the marginalized joint posterior probability distributions are almost identical between the analysis from [20] and our recovery run. Slight differences in the tails can be attributed to emulator accuracy as well as the different settings between both analyses mentioned above.

We also perform a test of  $\Lambda$ CDM constraints using an EDE emulator with a minimal amount of EDE. Contours are shown in Fig. 7.

<sup>11</sup>[https://flatironinstitute.org/chill/H21\\_data/](https://flatironinstitute.org/chill/H21_data/)

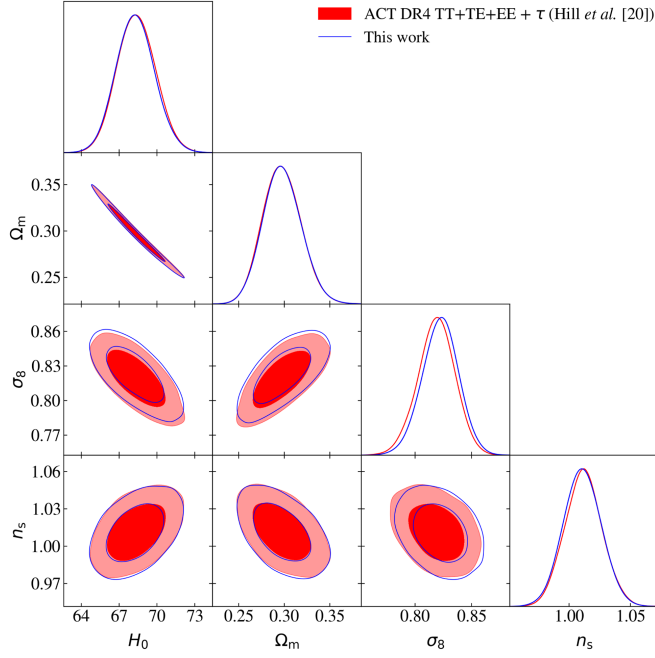


FIG. 7. Marginalized (1D and 2D) joint posterior probability distributions of  $\Lambda$ CDM parameters in fits of ACT DR4 CMB data in combination with a Gaussian prior on the optical depth. The blue contours use EDE emulators with minimal EDE content,  $f_{\text{EDE}} = 0.001$ . See text for details. The slight shift in  $\sigma_8$  is in the expected direction, and the positive degeneracy between  $f_{\text{EDE}}$  and  $\sigma_8$  could also be due to slightly different accuracy settings.

Overall, these results validate the use of the EDE emulators for the analysis of ACT DR4 CMB TT + TE + EE spectra.

#### 4. Planck 2018 TTTEE EDE constraints

For completeness, we reproduce results from [16] corresponding to the first column of their Table I. For this analysis, [16] uses CMB data from Planck PR3 including `planck_2018_lowl.TT`, `planck_2018_lowl.EE`, and `planck_2018_highl_plik.TTTEEE`, as well as a Gaussian prior on the Sunyaev-Zel'dovich components. While [16] carries out the analysis using the PLIK high- $\ell$  likelihood, we choose to use the native Python implementation available in Cobaya, i.e., `planck_2018_highl_plik.TTTEEE_lite_native`.<sup>12</sup>

The authors of [16] require a convergence criterion of  $R - 1 < 0.05$  and use an earlier version of `CLASS_EDE` than the one on which our EDE emulators are based. They consider one massive and two massless neutrinos and default `CLASS v2.8.2` settings for other cosmological and precision parameters, except for `P_k_max_h/Mpc` which they set to 20. Thus, our accuracy settings and convergence criterion are considerably more demanding than those of [16].

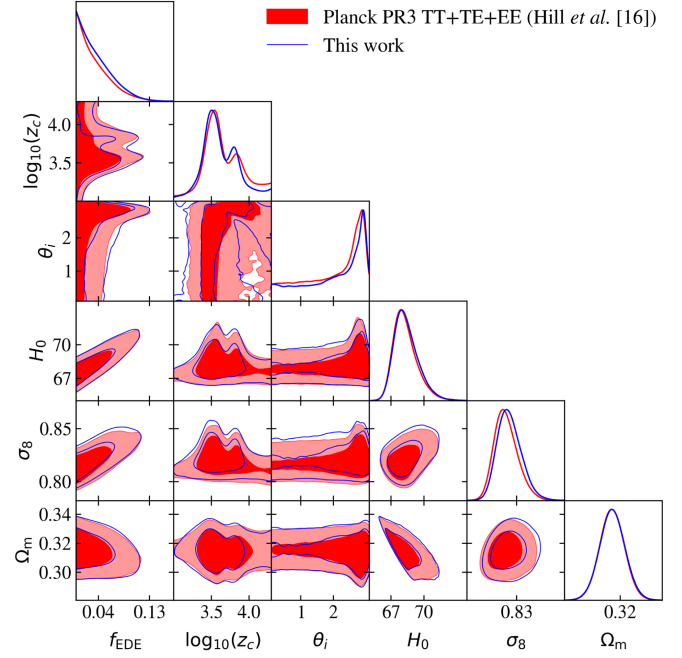


FIG. 8. Marginalized (1D and 2D) joint posterior probability distributions for Planck PR3 benchmark. See text for details.

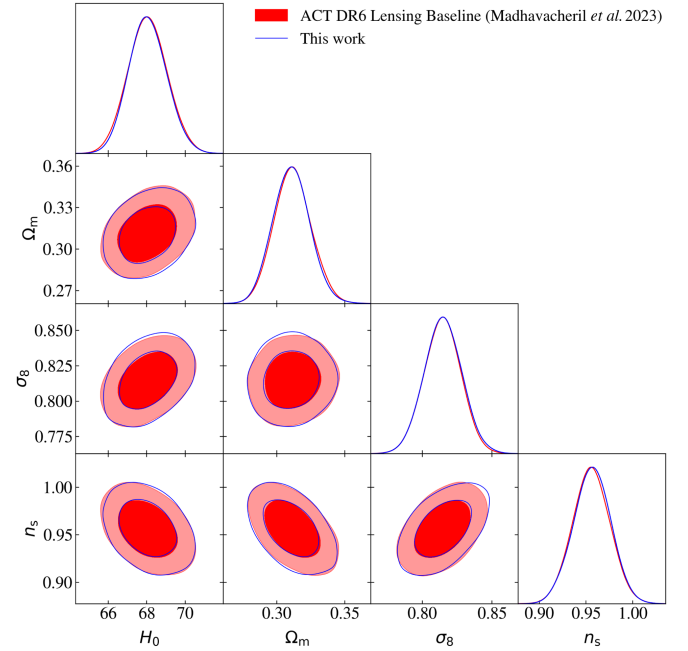


FIG. 9. Marginalized (1D and 2D) joint posterior probability distributions for ACT DR6 lensing benchmark. This includes pre-DESI BAO data. The blue contours use EDE emulators with minimal EDE content,  $f_{\text{EDE}} = 0.001$ . See text for details.

The chains from [16] are available online.<sup>13</sup> Analyzing these and excluding 50% of burn-in, we get  $R-1 = 0.02605$ . In comparison, excluding the same burn-in fraction,

<sup>12</sup>See <https://cobaya.readthedocs.io/likelihood/planck.html>.

<sup>13</sup>[https://www.simonsfoundation.org/flatiron/chill/H20/\\_data/](https://www.simonsfoundation.org/flatiron/chill/H20/_data/)

our chains have  $R - 1 = 0.00099$ . Corresponding contours are shown on Fig. 8. In spite of the differences mentioned above, both analyses match nearly perfectly. We get  $f_{\text{EDE}} < 0.0925$  (95% CL) (against 0.0908 from our reanalysis of the chains from [16]); we note that this is slightly different from the value quoted in their table, 0.087),  $\log_{10}(z_c) = 3.63 \pm 0.24$  (68% CL) [against  $\log_{10}(z_c) = 3.66^{+0.24}_{-0.28}$  from our reanalysis of the chains from [16]],  $\theta_i > 1.73$  (68% CL) (against 1.67 from our reanalysis of the chains from [16]),  $\Omega_m = 0.3146 \pm 0.0088$  (68% CL) (against  $0.3144 \pm 0.0086$  from our reanalysis of the chains from [16]),  $\sigma_8 = 0.8235^{+0.0096}_{-0.013}$  (68% CL) (against  $0.8202^{+0.0091}_{-0.013}$  from our reanalysis of the chains from [16]), and  $H_0 = 68.42^{+0.79}_{-1.3}$  km s<sup>-1</sup> Mpc<sup>-1</sup> (68% CL)

(against  $68.33^{+0.73}_{-1.3}$  from our reanalysis of the chains from [16]).

### 5. ACT DR6 lensing with EDE emulator $\Lambda$ CDM constraints benchmark

To test our EDE emulators on CMB lensing data, we perform a baseline ACT DR6 lensing analysis with EDE emulators and minimal amount of EDE. In particular, we set  $f_{\text{EDE}} = 0.001$ ,  $\theta_{i,\text{scf}} = 2.97$ , and  $\log_{10} z_c = 3.72$ . The data include DR6 and Planck lensing as well as pre-DESI BAO. Excluding 10% of burn-in, our chains have  $R - 1 = 0.00586$ . Contours are shown in Fig. 9.

- 
- [1] N. Aghanim *et al.* (Planck Collaboration), *Astron. Astrophys.* **641**, A6 (2020); **652**, C4(E) (2021).
- [2] L. Breuval, A. G. Riess, S. Casertano, W. Yuan, L. M. Macri, M. Romaniello, Y. S. Murakami, D. Scolnic, G. S. Anand, and I. Soszyński, *Astrophys. J.* **973**, 30 (2024).
- [3] L. Verde, T. Treu, and A. G. Riess, *Nat. Astron.* **3**, 891 (2019).
- [4] E. Di Valentino, O. Mena, S. Pan, L. Visinelli, W. Yang, A. Melchiorri, D. F. Mota, A. G. Riess, and J. Silk, *Classical Quantum Gravity* **38**, 153001 (2021).
- [5] W. L. Freedman, *Astrophys. J.* **919**, 16 (2021).
- [6] D. Scolnic, A. G. Riess, J. Wu, S. Li, G. S. Anand, R. Beaton, S. Casertano, R. Anderson, S. Dhawan, and X. Ke, *Astrophys. J. Lett.* **954**, L31 (2023).
- [7] W. L. Freedman *et al.*, *Astrophys. J.* **553**, 47 (2001).
- [8] W. L. Freedman and B. F. Madore, *J. Cosmol. Astropart. Phys.* **11** (2023) 050.
- [9] E. McDonough, J. C. Hill, M. M. Ivanov, A. La Posta, and M. W. Toomey, *J. Mod. Phys. D* **33**, 2430003 (2024).
- [10] V. Poulin, T. L. Smith, and T. Karwal, *Phys. Dark Universe* **42**, 101348 (2023).
- [11] V. Poulin, T. L. Smith, T. Karwal, and M. Kamionkowski, *Phys. Rev. Lett.* **122**, 221301 (2019).
- [12] M.-X. Lin, G. Benevento, W. Hu, and M. Raveri, *Phys. Rev. D* **100**, 063542 (2019).
- [13] P. Agrawal, F.-Y. Cyr-Racine, D. Pinner, and L. Randall, *Phys. Dark Universe* **42**, 101347 (2023).
- [14] M. Kamionkowski and A. G. Riess, *Annu. Rev. Nucl. Part. Sci.* **73**, 153 (2023).
- [15] T. L. Smith, V. Poulin, and M. A. Amin, *Phys. Rev. D* **101**, 063523 (2020).
- [16] J. C. Hill, E. McDonough, M. W. Toomey, and S. Alexander, *Phys. Rev. D* **102**, 043507 (2020).
- [17] M. M. Ivanov, E. McDonough, J. C. Hill, M. Simonović, M. W. Toomey, S. Alexander, and M. Zaldarriaga, *Phys. Rev. D* **102**, 103502 (2020).
- [18] G. D'Amico, L. Senatore, P. Zhang, and H. Zheng, *J. Cosmol. Astropart. Phys.* **05** (2021) 072.
- [19] A. La Posta, T. Louis, X. Garrido, and J. C. Hill, *Phys. Rev. D* **105**, 083519 (2022).
- [20] J. C. Hill, E. Calabrese *et al.*, *Phys. Rev. D* **105**, 123536 (2022).
- [21] V. Poulin, T. L. Smith, and T. Karwal, [arXiv:2302.09032](https://arxiv.org/abs/2302.09032).
- [22] A. Spurio Mancini, D. Piras, J. Alsing, B. Joachimi, and M. P. Hobson, *Mon. Not. R. Astron. Soc.* **511**, 1771 (2022).
- [23] B. Bolliet, A. S. Mancini, J. C. Hill, M. Madhavacheril, H. T. Jense, E. Calabrese, and J. Dunkley, *Mon. Not. R. Astron. Soc.* **531**, 1351 (2024).
- [24] B. Bolliet *et al.*, *EPJ Web Conf.* **293**, 00008 (2024).
- [25] J. Torrado and A. Lewis, *J. Cosmol. Astropart. Phys.* **05** (2021) 057.
- [26] G. Efstathiou, E. Rosenberg, and V. Poulin, *Phys. Rev. Lett.* **132**, 221002 (2024).
- [27] H. T. Jense, I. Harrison, E. Calabrese, A. S. Mancini, B. Bolliet, J. Dunkley, and J. C. Hill, *RAS Tech. Instrum.* **4**, rzaf002 (2025).
- [28] Y. Akrami *et al.* (Planck Collaboration), *Astron. Astrophys.* **643**, A42 (2020).
- [29] E. Rosenberg, S. Gratton, and G. Efstathiou, *Mon. Not. R. Astron. Soc.* **517**, 4620 (2022).
- [30] L. Pagano, J. M. Delouis, S. Mottet, J. L. Puget, and L. Vibert, *Astron. Astrophys.* **635**, A99 (2020).
- [31] F. J. Qu *et al.* (ACT Collaboration), *Astrophys. J.* **962**, 112 (2024).
- [32] M. S. Madhavacheril *et al.* (ACT Collaboration), *Astrophys. J.* **962**, 113 (2024).
- [33] N. MacCrann *et al.* (ACT Collaboration), *Astrophys. J.* **966**, 138 (2024).
- [34] Planck Collaboration, *Astron. Astrophys.* **641**, A8 (2020).
- [35] DESI Collaboration, *J. Cosmol. Astropart. Phys.* **02** (2025) 021.
- [36] F. Beutler, C. Blake, M. Colless, D. H. Jones, L. Staveley-Smith, L. Campbell, Q. Parker, W. Saunders, and F. Watson, *Mon. Not. R. Astron. Soc.* **416**, 3017 (2011).
- [37] A. J. Ross, L. Samushia, C. Howlett, W. J. Percival, A. Burden, and M. Manera, *Mon. Not. R. Astron. Soc.* **449**, 835 (2015).
- [38] S. Alam *et al.*, *Mon. Not. R. Astron. Soc.* **470**, 2617 (2017).
- [39] S. Alam *et al.*, *Phys. Rev. D* **103**, 083533 (2021).

- [40] D. Scolnic *et al.*, *Astrophys. J.* **938**, 113 (2022).
- [41] D. Brout *et al.*, *Astrophys. J.* **938**, 110 (2022).
- [42] A. Reeves, L. Herold, S. Vagnozzi, B. D. Sherwin, and E. G. M. Ferreira, *Mon. Not. R. Astron. Soc.* **520**, 3688 (2023).
- [43] S. Goldstein, J. C. Hill, V. Iršič, and B. D. Sherwin, *Phys. Rev. Lett.* **131**, 201001 (2023).
- [44] V. Poulin, T. L. Smith, and A. Bartlett, *Phys. Rev. D* **104**, 123550 (2021).
- [45] T. L. Smith, M. Lucca, V. Poulin, G. F. Abellan, L. Balkenhol, K. Benabed, S. Galli, and R. Murgia, *Phys. Rev. D* **106**, 043526 (2022).
- [46] S. K. Choi *et al.* (ACT Collaboration), *J. Cosmol. Astropart. Phys.* **12** (2020) 045.
- [47] S. Aiola *et al.* (ACT Collaboration), *J. Cosmol. Astropart. Phys.* **12** (2020) 047.
- [48] B. A. Benson *et al.* (SPT-3G Collaboration), *Proc. SPIE Int. Soc. Opt. Eng.* **9153**, 91531P (2014).
- [49] L. Herold, E. G. M. Ferreira, and E. Komatsu, *Astrophys. J. Lett.* **929**, L16 (2022).
- [50] A. Nygaard, E. B. Holm, S. Hannestad, and T. Tram, *J. Cosmol. Astropart. Phys.* **05** (2023) 025.
- [51] A. Nygaard, E. B. Holm, S. Hannestad, and T. Tram, *J. Cosmol. Astropart. Phys.* **11** (2023) 064.
- [52] A. Lewis, [arXiv:1910.13970](https://arxiv.org/abs/1910.13970).
- [53] M. Bonici, E. Baxter, F. Bianchini, and J. Ruiz-Zapatero, *Open J. Astrophys.* **7** (2024).
- [54] J. Lesgourgues, [arXiv:1104.2932](https://arxiv.org/abs/1104.2932).
- [55] D. Blas, J. Lesgourgues, and T. Tram, *J. Cosmol. Astropart. Phys.* **07** (2011) 034.
- [56] F. McCarthy, J. C. Hill, and M. S. Madhavacheril, *Phys. Rev. D* **105**, 023517 (2022).
- [57] S. Seager, D. D. Sasselov, and D. Scott, *Astrophys. J. Lett.* **523**, L1 (1999).
- [58] D. Scott and A. Moss, *Mon. Not. R. Astron. Soc.* **397**, 445 (2009).
- [59] J. Chluba, J. Fung, and E. R. Switzer, *Mon. Not. R. Astron. Soc.* **423**, 3227 (2012).
- [60] R. Consiglio, P. F. de Salas, G. Mangano, G. Miele, S. Pastor, and O. Pisanti, *Comput. Phys. Commun.* **233**, 237 (2018).
- [61] A. Mead, C. Heymans, L. Lombriser, J. Peacock, O. Steele, and H. Winther, *Mon. Not. R. Astron. Soc.* **459**, 1468 (2016).
- [62] J. Torrado and A. Lewis, *J. Cosmol. Astropart. Phys.* **05** (2021) 057.